PHYSICAL REVIEW B VOLUME 47, NUMBER 20 15 MAY 1993-II

Subpicosecond thermalization and relaxation of highly photoexcited electrons and holes in intrinsic and *p*-type GaAs and InP

U. Hohenester, P. Supancic, and P. Kocevar
Institut für Theoretische Physik, Karl-Franzens-Universität, A-8010 Graz, Austria

X. Q. Zhou
Max-Planck-Institut für Festkörperforschung, D-7000 Stuttgart 80, Germany

W. Kütt and H. Kurz
Institute of Semiconductor Electronics, Rheinisch-Westfälische Technische Hochschule Aachen, D-5100 Aachen, Germany

(Received 14 September 1992)

A combined experimental and theoretical investigation of the thermalization and relaxation of optically excited electrons and holes in intrinsic and *p*-type bulk GaAs and InP is presented. Using 50-fs and 2-eV laser-excitation pulses the hot-carrier dynamics was studied by the transient-absorption changes at 2 eV and by time-resolved luminescence spectroscopy, with a time resolution of 50–80 fs. The materials and doping levels were chosen to obtain, in combination with extensive ensemble Monte Carlo simulations, detailed information on intervalley and interband transfers of electrons and holes and on the effects of nonequilibrium optic phonons, of ionizing carrier–neutral-acceptor scatterings, and of dynamical screening of the various carrier-carrier interactions. Very good agreement between theory and experiment is found for the transient-absorption bleachings and the band-gap luminescence as functions of time and doping. For times beyond 500 fs the effective plasma-temperatures $T_{\rm eff}$, defined from the measured luminescence spectra, are well reproduced by theory. For shorter times, the calculated $T_{\rm eff}$ are systematically too high. This deviation is tentatively ascribed to effects of collisional broadening and band nonparabolicities.

I. INTRODUCTION

In view of the rapid development of electronic and optoelectronic semiconductor devices and of the continuing request for shorter switching and response times, the elucidation of the basic electronic processes in highly excited systems has for many years, besides its relevance for basic solid-state research, become of increasing practical importance. For example, the efficiency of recently proposed ultrafast electronic quantum-interference devices will be finally limited by phase-breaking scattering events such as carrier-carrier collisions, which, for moderate and high carrier densities and temperatures, are the fastest and dominant inelastic processes. Basic research on the intercarrier dynamics is also under way in connection with the exploration of future optoelectronic switching devices based on absorption changes induced by high-density photogenerated carrier plasmas in semiconductors.[1]

The history of such attempts started some 20 years ago, and since then good progress has been made, particularly in time-resolved luminescence and absorption spectroscopy of highly photoexcited bulk and microstructured semiconductors. These experimental achievements were complemented by the development of strongly improved computational techniques for hot-carrier transport calculations, and here most effectively by numerical Monte Carlo simulations of the corresponding internal and mutual thermalization and energy relaxation of the hot electrons and holes.[2–4] At first, the discussion centered on the individual contributions of the various types of carrier-carrier and carrier-phonon scatterings to the energy relaxation of the photoexcited carriers in the picosecond time domain. Controversial opinions were presented, e.g., about the relative role of optic-phonon disturbances and the free-carrier screening of long-range Coulombic interactions in polar semiconductors, stimulating the use of independent and complementary experimental techniques such as time-resolved Raman spectroscopy[5] and infrared spectroscopy of the free-carrier absorption of laser-pulse excited carriers.[6]

With the advent of subpicosecond laser spectroscopy, the problematics shifted to the discussion of the individual thermalization rates of photoexcited electrons and holes. Early experimental results at high excitation densities (around and above typically several 10^{18} electron-hole pairs per cm^3) and high excitation energies indicated thermalization times of the order of several 100 fs.[7] Within the last few years, however, a number of investigators found evidence suggesting much faster internal thermalization rates even at moderate carrier densities, at least for photoexcited quasi-two-dimensional electron-hole plasmas in quantum-well systems.[8] The present paper supports these earlier results by combining a systematic time-resolved hot-carrier spectroscopy of both intrinsic and variously *p*-doped bulk gallium arsenide and indium phosphide with a detailed theoretical analysis in the form of extended ensemble Monte Carlo simulations.

Laser pulses of 50-fs duration and 2-eV photon energy were used to excite valence electrons across the band gap and to monitor both the initial broadening of the photo-

 ©1993 The American Physical Society

generated band populations and the ensuing internal and mutual thermalization and energy relaxation of electrons and holes by detecting the time-resolved spectral luminescence and the transient bleaching of the samples around the energy of excitation. One of the reasons to choose InP as the second material was that for the 2-eV-excitation photons of our experiments the optical responses of the two materials differ mainly in the role of the electronic intervalley scatterings. In GaAs this intervalley dynamics is much more pronounced, because the majority of the photogenerated electrons in the central Γ valley of the conduction band are excited at energies larger than the threshold for transfers to secondary conduction-band valleys, while in InP all photogenerated electrons are excited at energies below this threshold. By comparing the otherwise similar optical-response scenarios in the two materials, one can obtain qualitative information on the comparative role of valley transfers in these materials. With this knowledge one can design specific experiments, which can give quantitative information on the strength of the Γ-*L* transfer rate in GaAs, which governs important electronic properties of this material, such as its negative differential conductivity and the transient velocity overshoot.

A wide range of excitation and doping densities was chosen to separate the relative contributions of the various carrier-carrier and carrier-acceptor interactions and to obtain additional information on the effects of nonequilibrium optic phonons and about the interband dynamics of holes, and here in particular about the relative contributions of phonon-assisted and nonphononic interband transitions.

II. EXPERIMENT

Our experimental setup was based on a colliding-pulse-mode locking laser system (pulse duration $t_p = 50$ fs and central wavelength 630 nm, i.e., photon energy $h\nu = 2$ eV). The beams were focused onto the sample with spot diameters ranging from 10 to 100 μm, thus changing the excited carrier density N_{exc}, averaged over the depth and lateral absorption profile, between several 10^{15} and several 10^{18} cm^{-3}. The InP and GaAs samples were grown by metal-organic chemical-vapor deposition and metal-organic molecular-beam epitaxy. The thin films for the transmission experiments were prepared by selective etching of substrate and intermediate edge-stop layers, e.g., $Ga_xIn_{1-x}As$ and $Al_xGa_{1-x}As$ layers, respectively. The samples used were epilayers for the luminescence studies and thin films of 100-nm thickness for the transmission measurements. All experiments were performed at room temperature.

In the time-resolved luminescence experiments, the emitted luminescence of the electron-hole pairs excited by one laser-pulse train was collected with a dispersion-free off-axis mirror system and focused onto a 1-mm BBO crystal. The second laser-pulse train was delayed by a stepper-motor delay stage and focused noncollinearly onto the nonlinear crystal to sample the luminescence transient by sum-frequency generation. The upconverted signal was dispersed by a monochromator and detected by single-photon counting. With this setup a time resolution better than 100 fs with high signal dynamics could be achieved over the whole spectral range.[9] The zero time delay was determined by the cross correlation between the stray laser light reflected from the sample. In order to achieve background-free luminescence spectra, the background was already subtracted during the measurement by chopping the laser excitation beam using a shutter.

The pump-probe experiments were performed with orthogonally polarized pump and probe pulses with equal beam diameters. The optical delay was accomplished using a retroreflector mounted on a shaker working at a rate of up to 200 Hz. The reflected and transmitted probe signals as well as two reference signals were detected with pin-Si photodiodes. Amplified difference signals were fed directly into a specially developed computer with a high-speed data-acquisition unit. This fast-scan technique allowed us to obtain relative signal changes of $\Delta R/R_0$ ($\Delta T/T_0$) of only a few 10^{-7} within several minutes signal-averaging time.[10] The absorption changes were evaluated from the experimental reflectivity and reflection transients by using thin-film equations. The zero time delay was determined by two-photon absorption in GaP platelets. This method was also used to define the temporal width of the laser pulse at 2 eV.

Some care had to be taken in the choice of the nominal excitation densities to be used in the simulation of the absorption data. For a given value of the maximal density at the surface and in the center of the excitation spot, the nominal density, which is treated as spatially homogeneous in the simulations, must have been averaged over of the lateral profile (conventionally assumed to be Gaussian) and over the exponential absorption-depth profile of the pump pulse. This gives about a factor-of-4 reduction in the nominal density, i.e., the average density is about a factor of 4 smaller than the maximum spot-center density at the surface. Non-perfect overlap of the pump and the probe beams at the sample surface and unsystematic errors in the pulse-energy and spot-size measurement may lead to densities which are about a factor of 8 smaller than the spot-center densities at the surface used in a preceding analysis of our transient absorption data.[11,12] In this connection we note that effects of spatial diffusion of the photoexcited carriers are practically negligible on the picosecond time scale of our experiments. For technical reasons the lower limit of spot-center excitation densities lay in the range of 10^{16} cm^{-3}.

Figure 1 shows the excitation scenario and the schematic band structure pertinent to our following analysis. Absorption of 2-eV photons from a 50-fs excitation (or pump) pulse involved distinct excitation channels from the heavy-hole, light-hole and spin-split-off valence bands. The time evolution of the photoexcited electrons and holes was monitored by measuring the spectrally resolved luminescence with time resolution of 80 fs and the temporal change of the absorption at 2 eV with a time resolution of 50 fs. The absorption changes are mainly caused by partial state filling of the three probed 2-eV absorption channels by the preceding 2-eV pump pulse. This results in a transient bleaching of the sample which directly reflects the buildup and decay of the photogen-

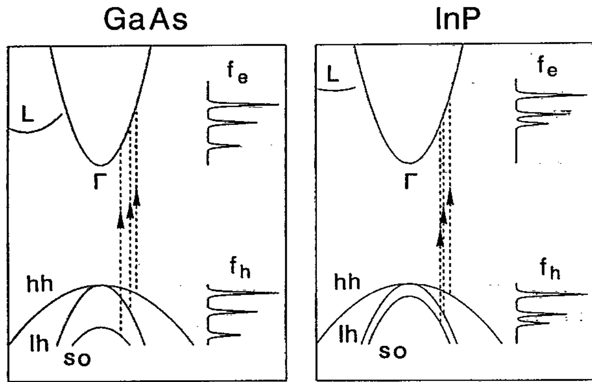

FIG. 1. Schematic band structures with optical excitation channels for GaAs and InP at room temperature.

erated band populations during and after the pump pulse. Time-resolved luminescence data involving lower frequencies yield the complementary information on the population of lower band regions and thereby on the down-relaxation of the photoexcited carriers and their accumulation near the band extrema.

Aside from the standard phase-space factors and optical transition amplitudes, the luminescence I_L and the bleaching contribution to the relative absorption change $\Delta\alpha/\alpha_0$ are determined by the sum over the participating transition channels of, respectively, the product $f_e^{(j)}f_h^{(j)}$ and the combination $-f_e^{(j)}-f_h^{(j)}$ of the distribution functions of the optically coupled electrons and holes. From Fig. 1 one notes the different role of the secondary conduction-band L valleys in GaAs and InP: for the 2-eV excitation photons the upper two heavy-hole (hh) and light-hole (lh) excitation peaks in the central Γ valley of GaAs lie above the Γ-L transfer threshold, while in InP all peaks lie rather far below this threshold.

III. THEORY: THE ENSEMBLE MONTE CARLO METHOD

A. The transport model

Our ensemble Monte Carlo (EMC) approach consisted of the **k**-space simulation of typically several tens of thousands of particles. For the following it is important to note that our conventional utilization of the EMC data to extract ensemble averages of single-particle energies and band occupations did not lead us out of the limits of the semiclassical Boltzmann equation, i.e., the description of ballistic particles with free flights between instantaneous, energy and momentum conserving scattering processes. We shall return to this point later.

By drawing on earlier assertions of a secondary role of band-structure details in a similar type of simulation,[13] we chose to neglect band anisotropies and nonparabolicities. The Γ-, L-, and X-valley electrons and heavy, light, and spin-split-off (sh) holes were therefore treated as particles with isotropic effective masses. An exception was the determination of the directly photogenerated band populations, where we included the effects of band anisotropies by using experimentally observed excitation linewidths.[14] We accounted for such spectral details and the time resolution of the experimental excitation and detection procedures through appropriate convolutions of the simulated carrier distributions in frequency and time. In this way nonclassical effects of collisional broadening[15] and band-gap renormalization[16] could, at least phenomenologically, be added to our single-particle treatment of the photogeneration and photorecombination process. As simple estimates showed a minor influence of the detailed convolution procedures, such additional broadening mechanisms were not included in the simulations. However, in connection with our following applications it is of interest that the neglect of line-shape corrections in the usual exponential fits of measured luminescence or absorption spectra will in general lead to an overestimate of the effective carrier temperatures.[17]

As recently estimated within a Maxwellian-carrier model of 2-eV laser-pulse excitation of GaAs,[18] our neglect of the nonparabolicity of the Γ valley may have resulted in too-high initial electron temperatures, typically on the (acceptable) order of 20 percent. Similarly, we do not expect any serious consequences of the replacement of the ellipsoidal satellite valleys by equivalent spherical valleys. As the dependence of the carrier relaxation on the detailed value of the effective mass $m_{\rm lh}$ of the light holes was small, we chose $m_{\rm lh}$ to closely reproduce the experimentally observed optically coupled band regions for our 2-eV-excitation and -probe pulses.[14] Here we assumed identical optical transition amplitudes for all three optical channels,[19] resulting in the partial channel contributions shown in Table I. The use of more realistic amplitudes from **k**·**p** calculations[14] would have yielded a slightly higher population of the hh-excitation channel and therefore slightly higher mean carrier energies.[20]

Our finding of a negligible dependence of the measured femtosecond bleachings on the relative orientation of the pump- and probe-pulse polarizations supports our neglect of the polarization-induced **k**-space anisotropy of the photogenerated and probed band populations. At the moderate excitation densities pertinent to our experiments, Auger processes[21] and free-carrier absorption[22]

TABLE I. Excitation energies ϵ (in eV) and relative weights w (in percent) of the three photogeneration channels used in the calculations.

	hh→Γ			lh→Γ			so→Γ		
Material	ϵ_Γ	$\epsilon_{\rm hh}$	$w_{\rm hh\to\Gamma}$	ϵ_Γ	$\epsilon_{\rm lh}$	$w_{\rm lh\to\Gamma}$	ϵ_Γ	$\epsilon_{\rm so}$	$w_{\rm so\to\Gamma}$
GaAs	0.50	0.07	0.46	0.35	0.23	0.32	0.16	0.07	0.23
InP	0.56	0.10	0.43	0.40	0.26	0.30	0.32	0.23	0.27

could be discarded.

The simulation contained all types of electron-electron (e-e), electron-hole (e-h), and hole-hole (h-h) scatterings and the interaction of electrons and holes with long-wavelength longitudinal-optic (LO) and transverse-optic (TO) phonons via the polar-optic (PO) and symmetry-allowed optic deformation potential (ODP) couplings as well as the dominant phonon-mediated intervalley (iv) and inter-valence-band transfers of electrons and holes. The phonon-assisted interband transfers were treated as ODP scatterings. We also included, as hitherto little explored energy-dissipation channels, ionizing carrier-neutral dopant scatterings[23] (see Appendix A) and non-phononic hh-lh interband transitions induced by e-h and h-h collisions[24] (see Appendix B). Here and in all further transition rates of holes we used Wiley's overlap corrections[25] for the predominant p-type symmetry of the valence-band wave functions. The overlap as well as the effects of degeneracy[26,27] and of optic-phonon disturbances[28] were included through use of suitable self-scattering techniques. In view of a recent criticism of the use of Wiley's approach in this type of analysis,[15] we tried several different overlap corrections, but found a minor influence on our final results.

The detailed treatment of the free-carrier screening of the polar-optic carrier-phonon couplings is known to be of secondary importance for the case of highly nonequilibrium LO phonons,[22] as realized in our experiments. We chose to use unscreened couplings as long as the multicomponent plasma frequency was smaller than the LO-phonon frequency and otherwise to screen the phonons by the Γ electrons using the time-dependent Thomas-Fermi susceptibility obtained from the instantaneous mean particle energy and population of the Γ valley.[29]

Our treatment of the free-carrier screening of the carrier-carrier (c-c) scatterings followed the conventional procedure of introducing collective plasma excitations. The remaining short-range interaction was treated by use of the long-wavelength limit of the static random-phase-approximation (RPA) dielectric function, i.e., by summing the time-dependent Thomas-Fermi susceptibilities of the separate hot-carrier subsystems. However, we accounted for the pronounced mass differences and the correspondingly different screening efficiencies of the various types of particles by allowing only particles of mass $\leq m_1$ to screen an interaction between two particles of mass m_1 and $m_2 \geq m_1$.

This static-plus-plasmonic approach, although containing plasmons, the self-consistent RPA prescription, and the mass criterion as dynamical ingredients, should be met with caution. The reason is that the description of scatterings with a strongly varying degree of inelasticity, such as collisions between carriers with equal or similar masses, would in principle require the use of a detailed dynamical screening theory. However, the implementation of a fully dynamical screening model into realistic transport calculations of the present type still proves to be beyond (at least conventional) present-day computer capacities.[29]

To further inquire into this matter, we investigated a simplified photoexcitation and thermalization scenario, consisting of only Γ-valley electrons, where all but the e-e scatterings were neglected. For this fictitious model system we compared the initial time evolution of the band population obtained from our quasistatic screening models with the results of a molecular-dynamics (MD) simulation (i.e., a simulation in $\mathbf{r}$ space), following the ideas of Ref. 30. Such an $\mathbf{r}$-space simulation replaces for each simulated electron its individual collisions with other electrons by the continuous action of the electric field produced by all the partner electrons in the ensemble. Although purely classical, this description should contain most ingredients of dynamical screening and should thereby lead to an increased efficiency of the e-e interaction as compared to its efficiency obtained in the conventional $\mathbf{k}$-space scattering formulations with one or the other form of static screening.

Figure 2 shows the results of this case study for the actual photoexcited Γ-valley populations in our high-excitation experiments, and Fig. 3 for the more perspicuous situation of a single δ-like excitation peak at time zero. We note that the molecular dynamics indeed yields a much faster initial broadening of the excitation spikes. Moreover, one easily recognizes the basic difference between the $\mathbf{r}$-space simulation and the kinetic approach. In the latter case and for sufficiently short times, a large fraction of carriers remains without any scatterings, resulting in a slow fading of the initial spikes, whereas the MD description leads to the immediate response of all carriers to the internal electric field and therefore to a very fast broadening of the photoexcitation peaks. In the kinetic description, on the other hand, each strongly in-

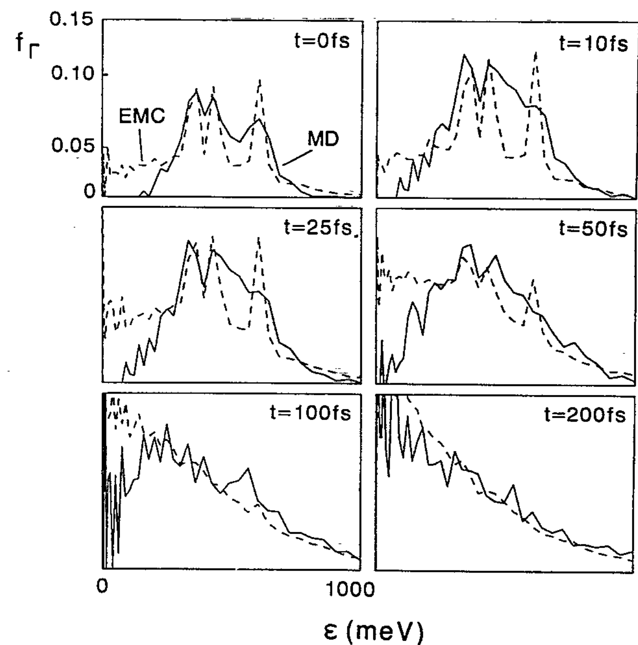

FIG. 2. Comparison of $\mathbf{k}$- and $\mathbf{r}$-space simulation of an isolated Γ-valley population in GaAs for the *realistic* excitation conditions of Fig. 1 and $N_{exc} = 1 \times 10^{18}$ cm^{-3}: solid line, MD; dotted line, EMC.

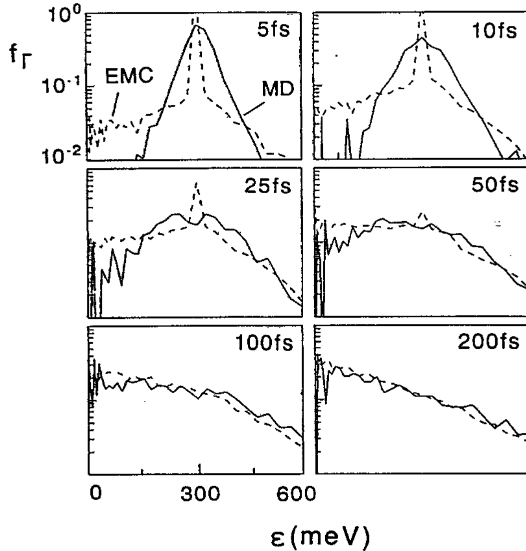

FIG. 3. Comparison of **k**- and **r**-space simulation of an isolated Γ-valley population in GaAs for an initially monoenergetic electron distribution of density $N_\Gamma = 1\times10^{18}$ cm^{-3}: solid line, MD; dotted line, EMC.

elastic scattering among the instantaneous *c*-*c* collisions is very effective in populating states near the band minimum and far above the excitation energies, whereas these extremal band regions are much later reached in the MD simulation, because of the less abrupt action of the total electronic field. This characteristic difference between the EMC and MD results will of course become less pronounced in realistic situations with additional inelastic-scattering mechanisms.

The persistence of photoexcitation spikes and the too-rapid filling of extremal band regions somehow pose a certain limitation to the use of kinetic transport calculations to reproduce detailed transient band occupations in the femtosecond regime. However, as seen from the eventual approach to a quasiexponential distribution, the **r**- and **k**-space simulations give very similar thermalization times, both of the order of 100 fs for the nominal densities of 2×10^{18} cm^{-3} of this example. These general conclusions are confirmed by recent results obtained from a similar critical comparison of **r**- and **k**-space methods in the description of highly photoexcited hot carriers in GaAs.[31] We believe that this good agreement is mainly due to the fact that for these high-excitation cases our theoretical model gives strongly reduced screening efficiencies because of the high kinetic carrier energies and the correspondingly reduced Thomas-Fermi susceptibilities. Indeed we have evidence from complementary studies of near-band-gap excitation that our modified Thomas-Fermi screening, in spite of its mass selectivity, becomes too strong when applied to a "cool" plasma.

In view of the considerable numerical expenditure in extending the MD technique to systems of oppositely charged particles and because of the great difficulties in treating degeneracy,[32] we have not followed the recent work of Elsässer *et al.*,[33,34] where the MD formulation of the electron-electron scattering was hybridized with an otherwise conventional **k**-space simulation of a nondegenerate, purely electronic plasma. Nevertheless, the results of our MD analysis (which can be viewed as a time-resolved demonstration of Boltzmann's *H*-theorem for a closed system of initially nonthermally distributed electrons[35]) did serve well as benchmarks for estimating possible uncertainties in our **k**-space simulation of the femtosecond intercarrier dynamics.

B. Examples

The material parameters used in our calculations are listed in Table II. As illustration of the effectivity of the various scattering mechanisms for the hot-carrier relaxation we compare the mean Γ-electron and heavy-hole energies as functions of time and the corresponding integrated energy-loss rates of Γ electrons for *i*- and *p*-InP in Fig. 4 and for *i*-GaAs at increasing excitation densities in Fig. 5.

The energy losses are divided into the contributions of the polar-optic interaction with LO phonons and the Γ-*L* intervalley and *e*-hh scatterings as the predominant dissipation channels. Most remarkably, the contributions of electron-plasmon processes are negligible, a result which is in contrast to the earlier findings of noticeable plasmon losses in similar simulations for single-component plasmas and low excitation energies.[36,37] The reason for this

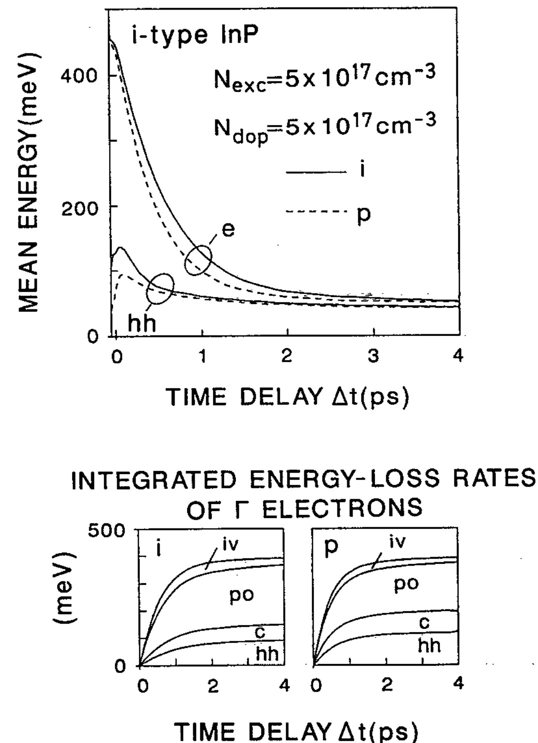

FIG. 4. Upper part: mean carrier energy of Γ electrons and heavy holes in *i*- and *p*-InP, for $N_{exc} = p = 5\times10^{17}$ cm^{-3}. Lower part: corresponding integrated rate for total mean energy loss per Γ electron divided into the partial losses to LO phonons (PO) and heavy holes (hh), and the contributions of the remaining electron-carrier scatterings (*c*) and of intervalley transfers (iv).

TABLE II. Material parameters used in the calculations.

Parameter	Unit	GaAs	InP
Band-gap energy at $T=300$ K (hh,Γ)	eV	1.423	1.339
(Γ,L)		0.280	0.635
(hh,lh)		0	0
(hh,so)		0.351	0.106
Crystal mass density	g/cm^{-3}	5.36	4.79
Effective mass m_Γ	m_0	0.067	0.078
m_L		0.222	0.4
m_X		0.58	0.58
$m_{\rm hh}$		0.45	0.45
$m_{\rm lh}$		0.102	0.12
$m_{\rm so}$		0.15	0.11
Lattice constant a_0	Å	5.642	5.45
iv-deformation potential $D_{\Gamma\to L}=D_{L\to\Gamma}$	eV/Å	5	2.3
$D_{\Gamma\to X}=D_{X\to\Gamma}$		5	2.3
iv-phonon energy $\hbar\omega_{\Gamma\to L}=\hbar\omega_{L\to\Gamma}$	meV	27.9	27.9
$\hbar\omega_{\Gamma\to X}=\hbar\omega_{X\to\Gamma}$		30	30
LO-phonon energy $\hbar\omega_{\rm LO}$	meV	36.8	43
TO-phonon energy $\hbar\omega_{\rm TO}$	meV	34.3	43
LO-relaxation time $\tau_{\rm LO}$ at $T=0$ K	ps	9	9
Optical deformation potential in L valley	eV/Å	3	3
hh,lh band		8.9	8.9
High-frequency dielectric constant ϵ_∞		10.92	9.52
Static dielectric constant ϵ_0		12.9	12.35
Number of L valleys		4	4
Number of X valleys		3	3

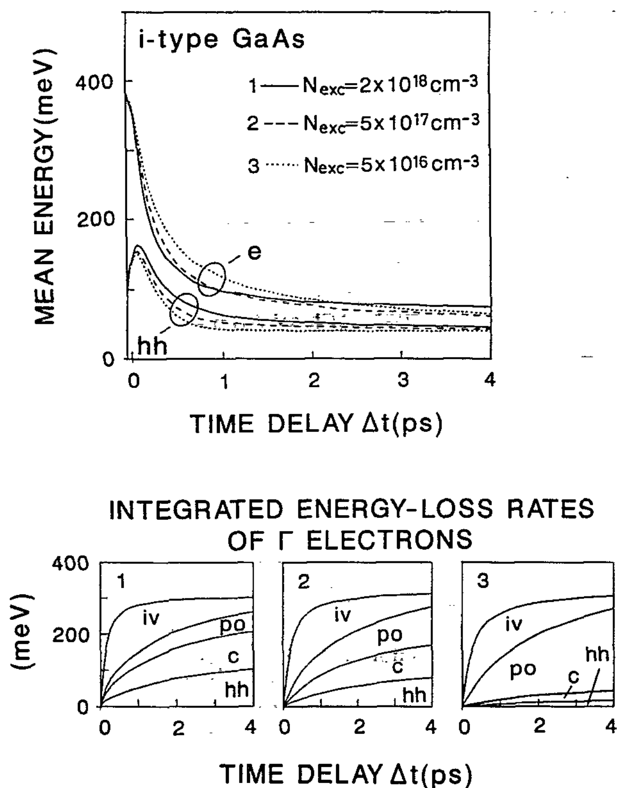

FIG. 5. As in Fig. 4, but for *i*-GaAs at three different excitation densities.

difference is that our calculations make allowance for the pronounced multicomponent nature of the carrier plasmas in the present experiments. Standard RPA theory[38] then results in a complete Landau damping of all modes, except those of very small wave vector. However, when properly treated as in nonequilibrium, these few long-lived modes turn out to become strongly heated and thereby lose their efficiency as temporary cooling reservoir for the carriers. This situation prevails in all our simulations, except in the cases of small excitation and large doping densities, which reflect the approach to the usual one-component plasma situation.

Both figures reveal the increasing importance of the $e\to h$ energy transfer with increasing hole concentration. In Fig. 4 the faster electron cooling for the p-doped material and the correspondingly faster initial increase of the mean hole energies from their starting values at the beginning of the excitation pulse are caused by the increased e-h scattering rate and also by the strong cooling efficiency of the initially cold doping background of holes. This increase of the relative importance of the e-hh channel is also seen from the integrated energy-loss rates in the lower part of the figure. In Fig. 5 the faster electron cooling and stronger heating of the holes with increasing excitation density are again due to the increase of the e-h scattering rate with the increasing hole concentration, as also seen from the increasing relative contribution of the e-h channel to the integrated energy losses. In agreement with previous work,[39–41] these calculations clearly demonstrate the efficiency of the weakly inelastic,

but very frequent e-h scatterings for the initial energy transfer from the hot Γ-valley electrons to the much cooler heavy holes, becoming, even for intrinsic materials, the leading power dissipation mechanism at the highest excitation densities.

Figure 6 depicts the temporal evolution of band populations for high excitation densities in intrinsic and in highly p-doped GaAs. The Γ-valley occupation is rapidly decreased due to the very fast initial transfers of electrons into the satellite valleys. For electrons with energies above the mean Γ-valley energy such a transfer reduces the mean Γ-valley energy. As the majority of the photoexcited electrons have energies above the Γ-L threshold, the initial valley transfers will act as a fast intermediate energy-loss mechanism for the central valley.

A significant overshoot of the hh-band population is calculated for p-doped materials, as shown in Fig. 6 for the case of p-GaAs. It is caused by the initial production of excess low-energy holes through the impact ionization of neutral acceptors by carriers with energies above the acceptor-ionization threshold (for GaAs taken as 25 meV; simple statistics shows that even at room temperature high-density doping levels lead to a substantial number of un-ionized acceptor atoms). Thereafter the cooling of the plasma reduces the number of such sufficiently energetic carriers, so that the recapture of holes by negative acceptors will eventually establish the thermal balance between free and bound holes. This overshoot of the hh population turned out to be the main cause of our experimental finding of a markedly faster onset of the band-edge luminescence in cases of highly p-doped materials at comparable excitation densities, as exemplified by the much slower onset obtained in our earlier simulations[12] which had not included acceptor ionizations. Moreover, the initial acceptor ionizations reduced the simulated mean Γ-electron energy $\langle E_\Gamma \rangle$ about typically ten percent during the first 200 fs, while at later times, beyond 500 fs, the inverse recapture processes resulted in a marginal backflow of energy to the carrier plasma. In this connection we note that the inclusion of interband transfers of holes through e-h collisions quite generally led to a lowering of $\langle E_\Gamma \rangle$ about a few percent in our simulations for both intrinsic and p-doped materials.

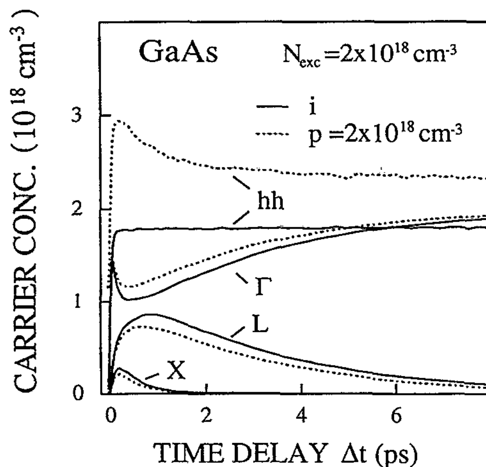

FIG. 6. Transient band occupations in i- and p-GaAs for $N_{exc}=2\times10^{18}$ cm^{-3} and $p=N_{exc}$.

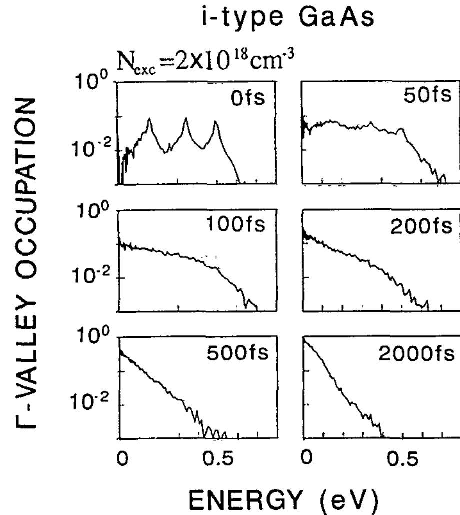

FIG. 7. Temporal evolution of the Γ-valley population in i-GaAs for the excitation conditions of Fig. 6.

The eventual return of the transferred electrons, typically after several picoseconds, then acts as an intermediate reheating of the Γ valley. This is demonstrated in Fig. 7, where the logarithmically plotted Γ-valley occupation as a function of time clearly shows, as deviations from the straight Maxwellians, the initial depletion of the upper band regions (at times $t=100$ and 200 fs) and their eventual refilling and overpopulation (at $t=500$ and 2000 fs).

IV. RESULTS: UPCONVERSION LUMINESCENCE

A. Transient luminescence spectra

We get very good agreement between our measurements and simulations for the time evolution of the band-gap luminescence in both GaAs and InP. Figure 8 clearly demonstrates the much faster onset of the band-

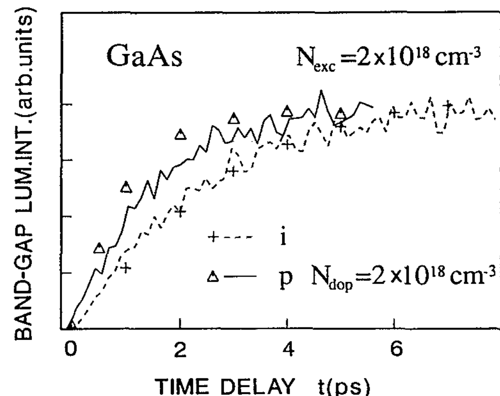

FIG. 8. Luminescence transients in i- and p-GaAs: band-gap luminescence for nominal excitation and doping densities of 2×10^{18} cm^{-3}.

gap luminescence for highly p-doped GaAs as compared to the case of the same excitation densities in undoped material. At comparable excitation and doping densities the main cause of this effect turns out to be the above-mentioned impact ionization of neutral acceptors and the resulting creation of extra free holes near the valence-band maximum, thereby raising the $f_e f_h$ product. For cases with high doping and low excitation density, neutral-acceptor scattering serves mainly as a fast additional energy-relaxation channel, reducing the number of electrons with sufficient energy for a Γ-L transfer. As more electrons relax directly towards the Γ-valley minimum, the rise time of the band-gap luminescence decreases with increasing doping level as shown in Fig. 9. This tendency is well reproduced by our simulations. Electronic energy losses to free holes play a similar role for the onset of the band-gap luminescence.[41] But careful comparisons between theory and experiment revealed that this scattering mechanism without inclusion of the neutral-acceptor ionizations could not reproduce the pronounced doping dependence of the experimental data. One should note that effects of an acceptor-induced enhancement of the density of states near the band extrema on the recombination rates are eliminated by the normalization of all luminescence intensities to the same maximum value in our figures.

The time-resolved luminescence spectra from higher band regions are particularly interesting. As shown in Fig. 10 for the case of highly excited i-GaAs, our simulated luminescence intensity for photon energies around $E_{gap}+200$ meV was extremely sensitive to the value of the Γ-L intervalley deformation potential $D_{\Gamma\text{-}L}$. We found that only a narrow range of $D_{\Gamma\text{-}L}=(5\pm0.5)$ eV/Å could simultaneously reproduce both the ($E_{gap}+200$ meV) luminescence and the cooling curves for various degrees of excitation and doping densities. This value is in agreement with a number of recent estimates[13,15] and also with the recent theoretical calculations of intervalley de-

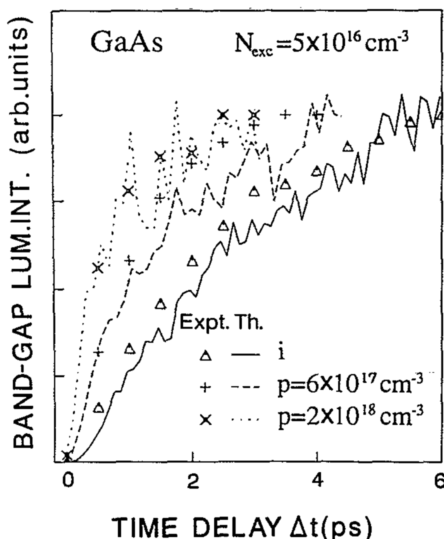

FIG. 9. Dependence of transient band-gap luminescence on p doping in GaAs for constant excitation density.

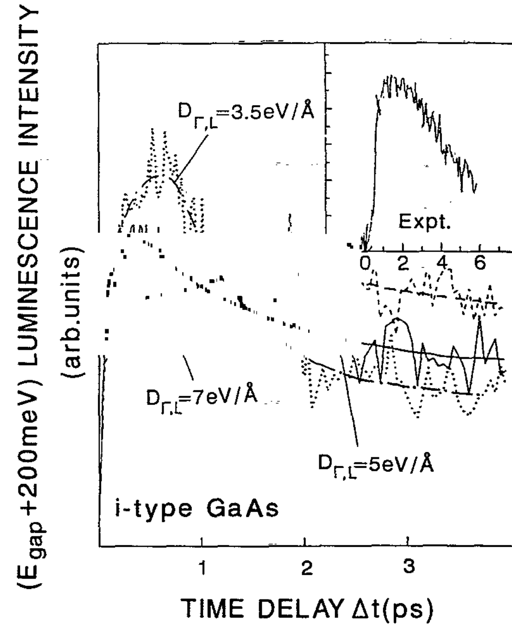

FIG. 10. Transient ($E_{gap}+200$ meV) luminescence in GaAs under the exciton conditions of Fig. 8, for different Γ-L intervalley deformation potentials $D_{\Gamma L}$. The electron energy E_Γ at the dominant Γ-hh recombination channel is 174 meV.

formation potentials.[42] It should be noted that a broad range of values for $D_{\Gamma\text{-}L}$ has been or is being proposed in the literature.[43] However, the transient spectral luminescence of our analysis seems at present the most precise experimental tool to determine $D_{\Gamma\text{-}L}$, when compared with its more indirect role in the optical or transport data used for its estimate in previous work.

We were not able to achieve the same quantitative agreement between theory and experiment for the luminescence data 320 meV above the gap; the simulated luminescence intensities were systematically too low. We ascribe the discrepancies to a nonthermal "hump" in the simulated carrier distributions due to a too-slow fading of the three excitation spikes during the first 100 fs. This will lead to an overestimate of the initial luminescence peak from these higher band regions. Normalizing the intensities to such an overestimated peak would then result in a rigid downshift of the luminescence curve at all later times. We cannot exclude the possibility that part of the discrepancy might be caused by effects of the Γ-valley nonparabolicity on the electronic intervalley dynamics. However, as the effects of nonparabolicity and of Γ-X valley transfers had been found to compensate each other under similar experimental conditions,[13] and since we found that (reasonable) variations of both the Γ-L and Γ-X intervalley couplings had little influence on the calculated $E_{gap}+320$ meV results, we expect such band-structure effects to be of secondary importance in our luminescence data.

B. Transient carrier cooling

A comparison of some typical experimental cooling curves with the theoretical results is shown in Fig. 11.

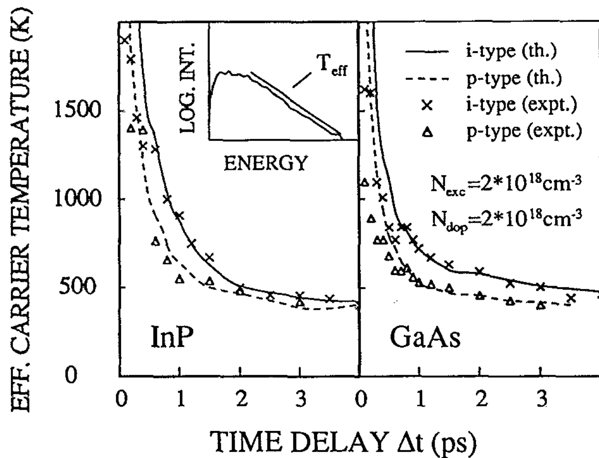

FIG. 11. Temporal evolution of effective carrier temperature in *i*- and *p*-InP and *i*- and *p*-GaAs for nominal excitation and doping densities of 2×10^{18} cm^{-3}. Inset: definition of instantaneous $T_{\rm eff}$ from quasiexponential shape of luminescence spectrum.

Here the concept of cooling is based on the notion of an effective plasma temperature $T_{\rm eff}$ which both experimentally and in the simulations is obtained from the near-exponential part of the time-resolved luminescence spectra. This procedure is schematically shown in the inset of the figure. Considering the dominant contribution $f_\Gamma f_{\rm hh}$ in the expression for the luminescence and using heated Maxwellians with temperatures T_Γ and $T_{\rm hh}$, respectively, one can easily verify that at the shortest times, when the Γ electrons are still much hotter than the holes, $T_{\rm eff}$ is a certain average of the individual electron and hole temperatures. At later times, when the Γ electrons have cooled down to temperatures comparable to that of the holes, $T_{\rm eff}$ more and more approaches T_Γ; this typically happens after T_Γ has dropped below 1000 K. At still longer times the establishment of a quasithermal equilibrium between electrons and holes would then be characterized by $T_{\rm eff}=T_\Gamma=T_{\rm hh}$. Since the internal thermalizations of the electron and hole subsystems occur in less than 100 fs, this description of the energy transfers within and out of the coupled electron and hole systems in terms of separate carrier temperatures and a corresponding effective plasma temperature is fully justified for times beyond a few hundred fs.

Figure 11 shows that the experimental cooling data for times beyond 500 fs are well described by the semiclassical kinetic transport model underlying our Monte Carlo analysis. This simulations revealed that in InP the cooling rate of the Γ electrons within this relaxation regime is noticeably reduced by the hot-phonon effect: the cooling efficiency of the most strongly coupling LO-phonon modes is reduced after their strong initial buildup by the photoexcited Γ electrons.[22] The upper part of Fig. 12 displays this LO-phonon amplification as function of phonon wave vector and time for our high-excitation experiment on *i*-InP. It is seen that the disturbance of the phonon distribution develops during the first picosecond after the excitation pulse, reaching a peak value of more than a tenfold amplification over the thermal-equilibrium value (≈ 0.23) for the long-wavelength modes. The lower part of Fig. 12 shows the pronounced increase of the simulated cooling rate when this phonon disturbance is neglected in the simulation. In GaAs the return of the initially transferred electrons back from the L valleys into high band regions of the Γ valley retards the Γ-valley cooling even more effectively than the hot-phonon effect. This sensitivity of cooling rates on the L-Γ transfer rate is crucial to define the range of acceptable $D_{\Gamma\text{-}L}$ values. The reduced cooling by the L-Γ return is also manifested by our experimental as well as theoretical finding that the dependence of the cooling rates on the excitation density in intrinsic material is stronger in InP. This reflects the pronounced dependence of the intraband relaxation dynamics of electrons and holes on the carrier densities (e.g., via e-h scatterings and LO-phonon heating) as compared to the minor density dependence of the electronic intervalley dynamics.

Quite generally, doping leads to a faster cooling, as seen in Fig. 11 for the case of comparable excitation and p-doping levels. This is consistent with the corresponding faster onset of the band-edge luminescence and is again caused by the presence of an initial background of cold holes and of a non-negligible number of neutral ac-

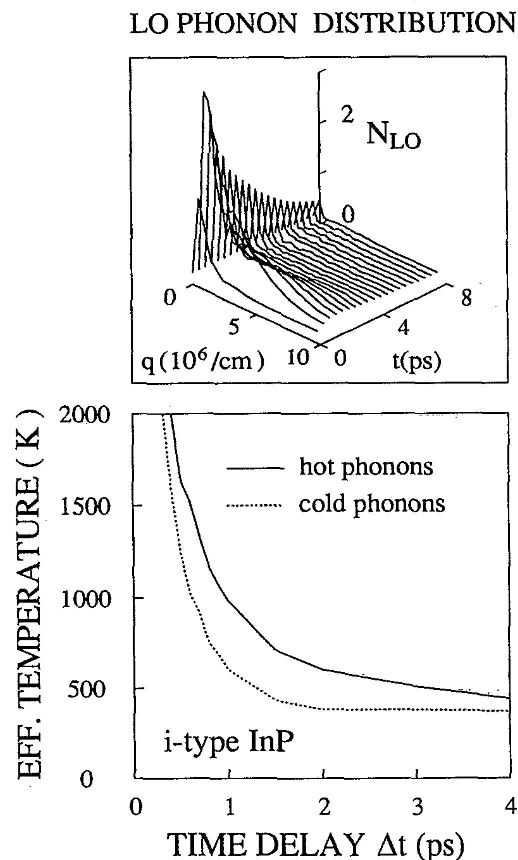

FIG. 12. Upper part: LO-phonon amplification in *i*-InP as function of phonon wave vector and time under the excitation conditions of Fig. 11. Lower part: corresponding "hot-phonon" effect on the plasma cooling.

ceptor atoms.

Despite the successful theoretical explanation of the luminescence data in the relaxation regime, a striking deviation remains for typically the first 500 fs. All effective temperatures derived from the simulations turn out to be systematically higher than the experimental T_{eff} values derived from the slope of the measured luminescence spectra. At present we have no satisfactory explanation for this discrepancy. In view of the rather phenomenological nature and qualitative determination of the effective plasma temperatures it might seem premature to regard these discrepancies as very serious. Moreover, various minor deficiencies of our transport model might sum up to the observed pronounced difference at ultrashort-time scales. In the following we shall consider several candidates for such possible causes.

As already mentioned in Sec. III, the inclusion of the Γ-valley nonparabolicity could at best reduce T_Γ about 20 percent, which does not suffice to explain the temperature differences seen in Fig. 11. Quite generally, we remark that effects of electron degeneracy are only noticeable for Γ-valley temperatures below typically 1000 K, and that variation, within reasonable limits, of the rates for Γ-*X* transfers in GaAs (Ref. 44) and for Γ-*L* transfers in InP, gave insignificant modifications of the cooling rates.

For InP the large theoretical T_{eff} values seem at first sight to be connected with the statement in Sec. III, that the initial broadening of the photoexcitation spikes in the **k**-space simulations is too slow: a faster broadening would help more Γ electrons to reach higher-lying energy thresholds for intervalley transfers, which in turn would effectively reduce the initial mean Γ-valley energy by removing particles high up in the band. However, this same argument does not apply to GaAs, where a faster broadening would indeed increase the number of Γ-*X* transfers at the highest energies, but would reduce the more frequent Γ-*L* events by transferring more electrons from energies above to energies below the Γ-*L* threshold. Moreover, the close agreement between EMC-simulated and molecular-dynamical thermalization times, of at most a few hundred fs, eliminates the possibility that the T_{eff} discrepancies may be caused by still not sufficiently thermalized EMC carrier distributions, because the discrepancies persist to times around 500 fs, when electrons and holds are perfectly Maxwellian. So, in view of the excellent results for all later times, we have to find modifications of our transport model which would increase the energy relaxation of the photoexcited carriers at the earliest times.

The fact that the largest T_{eff} discrepancies were found for heavily doped *p*-GaAs seems to indicate a decisive role of impurities: an increased initial electronic energy relaxation due to ionizations of uncontrolled neutral impurities might lead to a reduction of electronic transfers to satellite valleys. As a consequence, the direct intravalley down-relaxation of the electrons would speed up. This effect could be enhanced in doped and unintentionally compensated materials. However, our finding of rather small electronic energy losses through acceptor ionizations in all simulations of the *p*-doped materials eliminates this mechanism as a dominant cause for the high experimental cooling rates at the earliest times. But there remains the possibility of a faster carrier relaxation through impurity-induced enhancements of the electronic density of states near the Γ-valley minimum, whereas similar effects of an excitonic density-of-state enhancement can be ruled out for our room-temperature experiments.

Finally, we argue that a more effective cause of an increased electronic energy dissipation might be collisional broadening, for instance an initial enhancement of the number of small-**q** LO-phonon emissions. Some simplified cases have been recently studied in this context.[45,46] A complete model, however, for a realistic excitation scenario and including the counteraction of the correspondingly increased LO-phonon heating, has yet to be fully delineated. As already mentioned in Sec. III, a further helpful consequence of collisional broadening would be that an appropriate line-shape correction of the optical transition amplitudes will generally result in smaller carrier temperatures.[15,17] Here we believe that our numerical frequency convolutions should, at least qualitatively, include such effects.

The preceding discussion could not provide more than some suggestions for possible improvements of our description of the early cooling stage. But it nevertheless suggests that the kinetic approach for determining the initial carrier temperatures might be noticeably improved by use of a detailed band structure, by the inclusion of higher-order quantum corrections in the semiclassical scattering rates and by going beyond the independent-quasiparticle picture underlying our expressions for the optical transition rates. However, the implementation of these improvements into our elaborate EMC analysis was beyond our present computational capacities.

V. RESULTS: TRANSIENT ABSORPTION

Figure 13 shows transient bleachings caused by the partial state filling of the probed 2-eV absorption channels by the preceding 2-eV pump pulse. The most in-

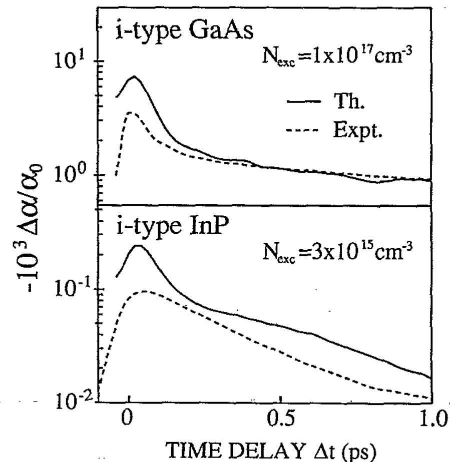

FIG. 13. Temporal evolution of absorption bleaching in *i*-GaAs and *i*-InP for high (1×10^{17} cm^{-3}) and low (3×10^{15} cm^{-3}) nominal excitation densities.

teresting feature of the calculated bleaching curves is the nonthermal hump obtained for the low-density bleaching experiment on InP. This specific feature in time domain demonstrates the temporal broadening of the initial excitation spikes. Its absence in the measured bleaching is the direct experimental evidence for thermalization times less than 100 fs at these low nominal densities of a few 10^{15} cm^{-3}. We have further confirmed this upper limit for thermalization times by comparing experimental bleaching data with theoretical bleaching values obtained by use of Maxwellians evaluated for the momentary simulated carrier energies and densities. These "Maxwellian" bleachings indeed fit the experimental curves very well, giving evidence for an actual thermalization within the time resolution of the experiments. The decay time of the transient bleaching curves, which is a direct measure of the cooling time of the hot carriers, slightly increases from 270 to 400 fs when increasing the excitation density from a few 10^{15} up to 10^{18} cm^{-3}. This is due to the hot-phonon effect, as verified numerically.

In GaAs, on the other hand, the hump in the time-resolved absorption data is due to Γ-L transfers. As shown in Fig. 13, even at high nominal excitation densities these extremely fast initial valley transfers can be well separated from the remaining relaxation rate. This feature is well reproduced by our simulations. However, it is important to note that only the properly corrected, i.e., nominal, densities lead to the quantitative agreement between experiment and theory.[47] In this way we were not forced to improve on the conventional Boltzmann picture, as was the case in a foregoing EMC analysis where a sort of self-consistent collisional broadening had to be included to explain very similar transient differential transmission data.[15] In view of the rather semiquantitative nature of our spatial averagings as well as of the conventional treatments of collisional broadening, this issue seems to be open, and it would be premature to make a strong point for or against the application of our present transport model to the ultrashort-time regime.

VI. SUMMARY

We have presented a combined experimental and theoretical analysis of highly photoexcited electrons and holes in intrinsic and p-doped bulk GaAs and InP for a wide range of excitation and doping levels. Laser pulses of 50 fs duration were used to excite valence electrons with 2 eV across the band gap and to monitor the initial broadening of the photogenerated band populations. The ensuing internal and mutual thermalization and the energy relaxation of electrons and holes was investigated by detecting the transient bleaching of the samples and by time-resolved spectral luminescence. The investigated materials and the experimental parameters were chosen to obtain, in combination with detailed ensemble Monte Carlo simulations, information on the intervalley-scattering rates of electrons and on the effects of dynamical free-carrier screening of the carrier-carrier interaction, inelastic carrier-acceptor scatterings, phononic as well as nonphononic interband transfers of holes, and nonequilibrium optic phonons and plasmons.

Very good agreement between theory and all luminescence data is found for the relaxation regime at times beyond typically 500 fs, where in InP the plasma cooling is found to be strongly retarded by hot-LO-phonon effects and in GaAs also by the return of initially $\Gamma \rightarrow L$ transferred electrons into the Γ valley. This latter dependence and the high sensitivity of the spectra luminescence from high band regions on the Γ-L dynamics allowed to determine the Γ-L intervalley deformation potential within the rather narrow range of 5 ± 0.5 eV/Å. Some systematic discrepancies between the experimental and simulated luminescence data for the initial thermalization regime remain, which may be attributed to deficiencies of the kinetic description at such short times.

This leaves us with a rather complete picture of the physical processes underlying our experimental data. In particular, and in agreement with earlier theoretical simulations and also with a recently published similar combined experimental and theoretical analysis of highly photoexcited GaAs, our analysis of the absorption bleaching gives evidence for an extremely fast broadening of the photogenerated band populations, followed by a very rapid thermalization of the individual electron and hole subsystems. For the highest carrier densities (2×10^{18} cm^{-3}) of our study, the corresponding time constants were found to be of the order of a few tens and a few hundred femtoseconds, respectively.

ACKNOWLEDGMENTS

Our thanks are due to U. Lemmer, P. Lugli, and L. Rota for many helpful discussions.

APPENDIX A

In this section we derive scattering rates for the ionization of neutral (monovalent) acceptors or donors and for the reverse carrier capture processes. Restricting ourselves to the simplest possible semiquantitative description, we assume that these processes only involve the 1s ground state with binding energy E_B. Denoting the concentration of neutral and charged donors or acceptors with N^0, N^+, and N^- and taking the spin degeneracy of the ground state into account, using golden-rule expressions for the transition rates involving the ground state and the three participating (plane-wave) free-carrier states and performing one momentum integration with help of the energy-conserving δ function, we arrive at the following expressions for the ionization and capture rates induced by a particle of wave vector $\mathbf{k}_1$:

$$P_{\rm ion}(\mathbf{k}_1)=\frac{2^6e^4m_2}{\hbar^3\pi\epsilon_0^2}\frac{N^0}{a_0^5}\int d^3k_1'\frac{1}{(K^2+\beta^2)^2}\Theta\left[\frac{\hbar^2(k_1^2-k_1'^2)}{2m_1}-E_B\right] \times\left[\frac{1}{6K}\left[\frac{1}{y_1^3}-\frac{1}{y_2^3}\right]+\frac{2k_{2,0}'}{(a_0^{-2}+k_{2,0}'^2)^4}-\frac{1}{K(a_0^{-2}+k_{2,0}'^2)^2}\left[\frac{1}{y_1}-\frac{1}{y_2}\right]\right], \tag{A1}$$

$$P_{\mathrm{cap}}(\mathbf{k}_1)=\frac{2^7 e^4 m_2}{\hbar^3\pi\epsilon_0^2}\frac{2N^{\pm}}{a_0^5}\int d^3k_1'\frac{f(k_{2,0}')}{(K^2+\beta^2)^2}\Theta\left[\frac{\hbar^2(k_1'^2-k_1^2)}{2m_1}-E_B\right]$$
$$\times\left[\frac{1}{6K}\left[\frac{1}{y_1^3}-\frac{1}{y_2^3}\right]+\frac{2k_{2,0}'}{(a_0^{-2}+k_{2,0}'^2)^4}-\frac{1}{K(a_0^{-2}+k_{2,0}'^2)^2}\left[\frac{1}{y_1}-\frac{1}{y_2}\right]\right], \tag{A2}$$

with

$$K=|\mathbf{k}_1-\mathbf{k}_1'| , \tag{A3}$$

$$y_{1,2}=a_0^{-2}+(K\mp k_{2,0}')^2 , \tag{A4}$$

and

$$k_{2,0}'^{\,\mathrm{ion,cap}}=[(2m_2)(\pm k_1^2/2m_1\mp k_1'^2/2m_1-E_B/\hbar^2)]^{1/2} , \tag{A5}$$

where a_0 denotes the effective Bohr radius, β the mass-selected hot-carrier screening parameter discussed in Sec. III, and Θ the step function. From the integrands in Eqs. (A1) and (A2) one obtains the various differential cross sections determining the final states in each simulated scattering event.

APPENDIX B

The energy-loss rates involving carrier-induced heavy-hole–light-hole transitions were first obtained by Ref. 24. For our ensemble Monte Carlo application these complicated expressions can be strongly simplified by first neglecting the overlap corrections [Eq. (2) in Ref. 24] in the total scattering rates and thereafter including them through a self-scattering technique.[15] Then the total rate per unit volume without overlap correction, with the state indices 2 and 2′ for the transferring hole, is given by

$$P_{\mathrm{tot}}(k_1)=\frac{2}{(2\pi)^3}\int d^3k_2\,\delta(E_{\mathrm{fin}}-E_{\mathrm{in}})f(k_2)\times\Theta\left[k_r^2-\frac{\mu_{12'}}{\bar{\mu}_{22'}}k_2^2\right]\times\left[\frac{4\pi e^4\mu_{12'}}{\epsilon_0^2\hbar^3 k_r}\frac{q_2^2-q_1^2}{(\beta^2+q_1^2)(\beta^2+q_2^2)}\right], \tag{B1}$$

with

$$\mu_{12'}=\frac{m_1 m_{2'}}{m_1+m_{2'}} , \tag{B2}$$

$$\bar{\mu}_{22'}=\frac{m_2 m_{2'}}{m_2-m_{2'}} , \tag{B3}$$

$$\mathbf{k}_r=\frac{m_{2'}}{m_1+m_{2'}}\mathbf{k}_1-\frac{m_1}{m_1+m_{2'}}\mathbf{k}_2 , \tag{B4}$$

$$q_{1,2}=k_r\pm\left[k_r^2-k_2^2\frac{\mu_{12'}}{\bar{\mu}_{22'}}\right]^{1/2} , \quad m_2>m_{2'} , \tag{B5}$$

$$q_{1,2}=\left[k_r^2-k_2^2\frac{\mu_{12'}}{\bar{\mu}_{22'}}\right]^{1/2}\mp k_r , \quad m_2<m_{2'} , \tag{B6}$$

where Θ denotes the step function. The corresponding differential scattering cross sections determining the final states are obtained from the integrand in Eq. (B1).

[1] J. H. Collet and M. Pugnet, Phys. Status Solidi B **146**, 393 (1988).

[2] *Proceedings of the 5th International Conference on Hot Carriers in Semiconductors, Boston, 1987,* edited by J. Shah and G. J. Iafrate (Pergamon, New York, 1988); Solid-State Electron. **31** (1988).

[3] *Proceedings of the 6th International Conference on Hot Carriers in Semiconductors, Phoenix, 1989,* edited by D. K. Ferry and L. A. Akers (Pergamon, New York, 1989); Solid-State Electron. **32** (1989).

[4] *Proceedings of the 7th International Conference on Hot Carriers in Semiconductors, Nara, 1991,* edited by C. Hamaguchi and M. Inoue (Hilger, Bristol, 1992); Semicond. Sci. Technol. **7** (1992).

[5] J. A. Kash, J. M. Hvam, J. C. Tsang, and T. F. Kuech, Phys. Rev. B **38**, 5776 (1988).

[6] T. Elsässer, R. J. Bäuerle, and W. Kaiser, Phys. Rev. B **40**, 2976 (1989).

[7] C. W. W. Bradley, R. A. Taylor, and J. F. Ryan, Solid-State Electron. **32**, 1173 (1989).

[8] S. M. Goodnick, P. Lugli, W. H. Knox, and D. S. Chemla, Solid-State Electron. **32**, 1737 (1989).

[9] X. Q. Zhou, Ph.D. thesis, Rheinisch-Westfälische Technische Hochschule, Aachen, 1991.

[10] M. M. Strahnen, W. Kütt, and H. Kurz, in *Proceedings of the International Conference on VME-bus in Research,* edited by C. Eck (North-Holland, Amsterdam, 1988), p. 69.

[11] X. Q. Zhou, G. C. Cho, U. Lemmer, W. Kütt, K. Wolter, and H. Kurz, in *Proceedings of the 6th International Conference on Hot Carriers in Semiconductors, Phoenix, 1989,* edited by D. K. Ferry and L. A. Akers (Pergamon, New York, 1989); Solid-State Electron. **32**, 1591 (1989).

[12] U. Hohenester, P. Supancic, P. Kocevar, X. Q. Zhou, U. Lemmer, G. C. Cho, W. Kütt, and H. Kurz, in *Proceedings of the 7th International Conference on Hot Carriers in Semiconductors, Nara, 1991* (Ref. 4); Semicond. Sci. Technol. B **7**, 176 (1992).

[13] J. Shah, B. Devaud, T. C. Damen, W. T. Tsang, A. C. Gos-

sard, and P. Lugli, Phys. Rev. Lett. **59**, 2222 (1987).
[14]G. Fasol, W. Hackenberg, H. P. Hughes, K. Ploog, E. Bauser, and H. Kano, Phys. Rev. B **31**, 1461 (1990).
[15]D. W. Bailey, C. J. Stanton, and K. Hess, Phys. Rev. B **42**, 3423 (1990).
[16]J. M. Wiesenfeld and A. J. Taylor, Phys. Rev. B **34**, 8740 (1986).
[17]J. H. Collet, W. W. Rühle, M. Pugnet, K. Leo, and A. Million, Phys. Rev. B **40**, 12 296 (1989); W. W. Rühle, J. Collet, M. Pugnet, and K. Leo, in *Condensed Systems of Low Dimensionality*, edited by J. L. Beeby *et al.* (Plenum, New York, 1991), p. 61.
[18]T. Gong, P. M. Fauchet, J. Young, and P. J. Kelly, Phys. Rev. B **44**, 6542 (1991).
[19]H. B. Bebb and E. W. Williams, in *Semiconductors and Semimetals*, edited by R. K. Willardson and A. C. Beer (Academic, New York, 1972), Vol. 8, p. 181.
[20]W. Hackenberg (private communication).
[21]O. Strauss, W. Rühle, and K. Köhler (unpublished).
[22]W. Pötz and P. Kocevar, Phys. Rev. B **28**, 7040 (1983).
[23]D. Snoke, W. Rühle, Y.-C. Lu, and E. Bauser, Phys. Rev. Lett. **68**, 990 (1992).
[24]F. Young, P. Kelly, and N. L. Henry, Phys. Rev. B **36**, 4535 (1987).
[25]J. D. Wiley, Phys. Rev. B **4**, 2485 (1971).
[26]S. Bosi and C. Jacoboni, J. Phys. C **9**, 315 (1976).
[27]P. Lugli and D. K. Ferry, Phys. Rev. Lett. **56**, 1295 (1986).
[28]P. Lugli, P. Bordone, L. Reggiani, M. Rieger, P. Kocevar, and S. M. Goodnick, Phys. Rev. B **39**, 7852 (1989).
[29]J. H. Collet, Phys. Rev. B **39**, 7659 (1989).
[30]C. Jacoboni, in *Proceedings of the 13th International Conference on the Physics of Semiconductors*, edited by G. Fumi (North-Holland, Amsterdam, 1976), p. 1195.
[31]L. Rota and D. K. Ferry (unpublished).
[32]A. M. Kriman, R. P. Joshi, M. J. Kann, and D. K. Ferry, in *Proceedings of the 7th International Conference on Hot Carriers in Semiconductors, Nara, 1991* (Ref. 4); Semicond. Sci. Technol. B **7**, 243 (1992).
[33]T. Elsässer, J. Shah, L. Rota, and P. Lugli, in *Proceedings of the 7th International Conference on Hot Carriers in Semiconductors, Nara, 1991* (Ref. 4); Semicond. Sci. Technol. B **7**, 144 (1992).
[34]T. Elsässer, J. Shah, L. Rota, and P. Lugli, Phys. Rev. Lett. **66**, 1757 (1991).
[35]S. M. Goodnick, in *Spectroscopy of Semiconductor Microstructures*, edited by G. Fasol, A. Fasolino, and P. Lugli (Plenum, New York, 1989), p. 561.
[36]L. Rota, P. Poli, C. Jacoboni, and P. Lugli, in *Proceedings of the 20th International Conference on the Physics of Semiconductors*, edited by E. M. Anastassakis and J. D. Joannopoulos (World Scientific, Singapore, 1990), p. 2534.
[37]L. Rota and P. Lugli, in *Proceedings of the 7th International Conference on Hot Carriers in Semiconductors, Nara, 1991* (Ref. 4); Semicond. Sci. Technol. B **7**, 180 (1992).
[38]H. Sato and Y. Hori, Phys. Rev. B **36**, 6033 (1987).
[39]Marion Asche and O. G. Sarbei, Phys. Status Solidi B **126**, 607 (1984).
[40]W. Pötz, Phys. Rev. B **36**, 5016 (1987).
[41]R. P. Joshi, R. O. Grondin, and D. K. Ferry, Phys. Rev. B **42**, 5685 (1990).
[42]S. Zollner, S. Gopalan, and M. Cardona, Solid State Commun. **76**, 877 (1990).
[43]For exhaustive compilations of proposed Γ-L deformation potentials see Refs. 13 and 14.
[44]D. N. Mirlin, I. Ya. Karlik, and V. F. Sapega, Solid State Commun. **65**, 171 (1988).
[45]F. Rossi and C. Jacoboni, in *Proceedings of the 7th International Conference on Hot Carriers in Semiconductors, Nara, 1991* (Ref. 4); Semicond. Sci. Technol. B **7**, 383 (1992).
[46]K. Kral, Phys. Status Solidi B **170**, 537 (1992).
[47]See, e.g., our earlier attempt in Ref. 12, where the spot-center densities at the surface were used as nominal densities.